International Journal of Nanomedicine

Dovepress
Taylor & Francis Group

Open Access Full Text Article

ORIGINAL RESEARCH

Internal-External Homologous Drug-Loaded Exosome-Like Nanovesicles Released from Semi-IPN Hydrogel Enhancing Wound Healing of Chemoradiotherapy-Induced Oral Mucositis

Xiangjuan Wei[1,*], Mengyuan Wang[1,*], Xiaocong Dong[1], Yichen He[1], Wenbin Nan[1], Shenglu Ji[1], Mengyuan Zhao[1], Haodang Chang[1], Hongliang Wei[2], Dan Ding[3], Hongli Chen[1]

[1]Clinical Medical Center of Tissue Engineering and Regeneration, The Third Affiliated Hospital, School of Life Science and Technology, Xinxiang Medical University, Xinxiang, Henan, People's Republic of China; [2]School of Chemistry and Chemical Engineering, Henan University of Technology, Zhengzhou, Henan, People's Republic of China; [3]Key Laboratory of Bioactive Materials for the Ministry of Education, College of Life Sciences, Nankai University, Tianjin, People's Republic of China

*These authors contributed equally to this work

Correspondence: Hongli Chen, Clinical Medical Center of Tissue Engineering and Regeneration, The Third Affiliated Hospital, School of Life Science and Technology, Xinxiang Medical University, Xinxiang, Henan, People's Republic of China, Email chenhlhl@126.com

Background: Oral mucositis (OM) is a common acute side effect among patients undergoing chemotherapy and/or radiotherapy, with complex pathogenesis and limited current treatment efficacy. *Rabdosia rubescens*, a traditional Chinese herb, contains oridonin (ORI) with antibacterial and anti - inflammatory properties. However, ORI's poor solubility and low bioavailability hamper its clinical use. Medicinal plant - derived exosome - like nanovesicles (ENs) are emerging as a promising drug delivery system for wound repair. This study aimed to develop a novel therapeutic approach.

Methods: We fabricated internally-externally homologous drug-loaded exosome-like nanovesicles (ORI/ENs) derived from *Rabdosia rubescens* and encapsulated them in a semi-interpenetrating network hydrogel system (ORI/ENs/Gel) to repair chemoradiotherapy-induced OM. The morphology, biocompatibility, and antibacterial properties were evaluated. Moreover, the proliferative and migratory capacity were measured using L929 cells. In addition, the pro-healing effects and the underlying molecular mechanisms of ORI/ENs/Gel were assessed in vivo.

Results: ENs were extracted and purified from *Rabdosia rubescens* by sequential ultra-centrifugations. The encapsulation efficiency (EE) and loading capacity (LC) of ORI in ORI/ENs were 76.4 ± 3.2% and 9.21 ± 0.45%, respectively, suggesting that ENs had a high loading efficiency for homologous drug ORI. The evaluation of toxicity and antibacterial effects has been proven that ORI/ENs has biocompatibility and antibacterial properties. In vivo, ORI/ENs/Gel promoted collagen deposition, targeted NLRP3 to reduce inflammation, and accelerated OM wound healing.

Conclusion: The hydrogel composite incorporating internally-externally homologous drug-loaded ENs offers the potential to provide targeted therapy, improve bioavailability, and promote efficient healing of the OM.

Keywords: chemoradiotherapy-induced oral mucositis, exosome-like nanovesicles, oridonin, hydrogel, NLRP3

Introduction

Oral mucositis (OM) is an acute adverse effect experienced by patients undergoing chemotherapy and/or radiotherapy. It is characterized by a complex molecular pathogenesis that involves damage to the epithelium and microvasculature, chronic inflammation, and oral microbial infections.[1,2] OM can lead to significant pain, discomfort, and difficulties in eating and speaking, ultimately diminishing the quality of life for affected patients.[3,4] Nearly 40% of patients receiving chemotherapy develop OM, and this proportion increases to 90% among those undergoing both chemotherapy and

Received: 26 November 2024
Accepted: 21 March 2025
Published: 4 April 2025

Graphical Abstract

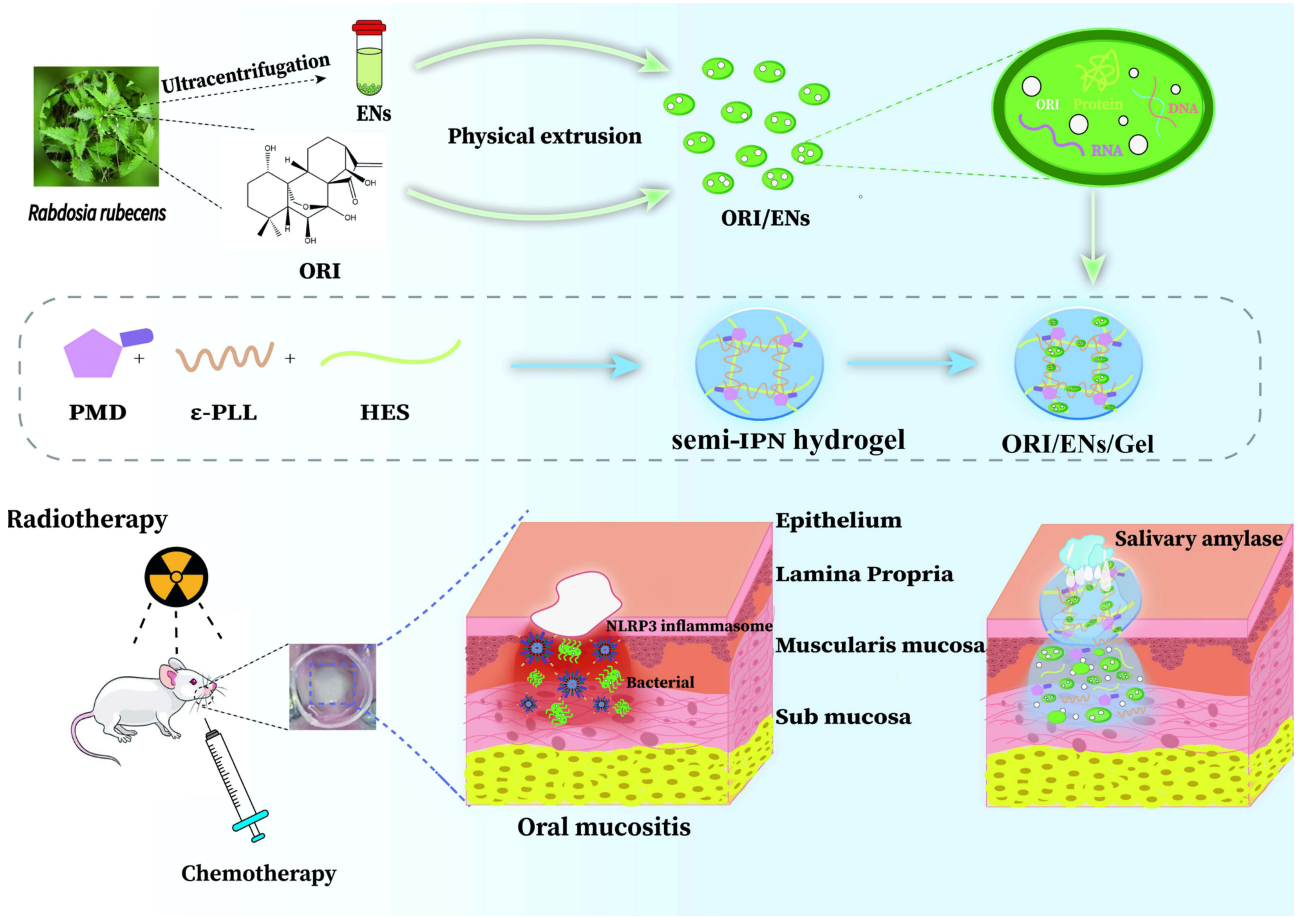

radiotherapy. Furthermore, 19% of these patients may need to suspend their anti-tumor therapy due to severe oral mucositis, which can result in a reduced quality of life, poor prognosis, and even shorter survival times.[5] Due to the complex and dynamic oral microenvironment, the efficacy of the current treatments is encounters several challenges, including increased infection rates and poor drug absorption and distribution.[6,7] Anti-infection and anti-inflammation are the primary objectives in promoting healing for OM, yet there is a notable absence of effective topical drug therapies for this condition.

In recent years, exosome-like nanovesicles (ENs) secreted by nearly all cell types have been investigated as a safe, biocompatible, and biodegradable drug delivery system, demonstrating significant potential for therapeutic applications.[8–12] Dependent on their ability to carry nucleic acids, proteins, and lipids, ENs are involved in almost all processes of wound repair, including anti-inflammatory responses, pro-collagen deposition, cell proliferation and migration, and pro-angiogenesis.[13–16] In addition, ENs derived from medicinal plants were expected to maintain the pharmacological activity of their parent compounds.[17] *Rabdosia rubescens*, a traditional Chinese herbal medicine, contains multiple natural active compounds, such as oridonin (ORI), which has been shown to exert diverse biological functions, including antibacterial, anti-inflammatory, anti-cancer, and oral inflammation or cancer-assisted treatment.[18] Thus, it is suggested that ENs derived from *Rabdosia rubescens* possess similar biological activities and play a pivotal role in pro-oral mucosal healing.

Recent research has demonstrated that ORI directly targets the NLRP3 inflammasome and specifically inhibits its activation. Furthermore, ORI and its structural analogs may have potential therapeutic roles in diseases associated with

NLRP3 dysregulation. ORI can also inhibit the activity of NF-κB and MAPK, thereby suppressing the secretion of inflammatory cytokines such as tumor necrosis factor-alpha (TNF-α) and interleukin-6 (IL-6).[19] However, the clinical application of ORI has been limited due to its poor water solubility and low bioavailability.[20,21] The use of a nano-drug delivery system can enhance the solubility of drugs and improve their bioavailability, thereby increasing their clinical utility.[22,23] Since the outer carriers of ENs and ORI (ORI/ENs) are derived from the same source plant, synergistic effects may be achieved, further enhancing their pharmacological activity. Consequently, we hypothesized that ORI/ENs could exert anti-inflammatory effects and enhance wound healing in chemotherapy/radiotherapy-induced OM by inhibiting the expression of NLRP3.

Hydrogels can protect oral mucosal wounds, alleviate pain, improve drug bioavailability, and exhibit anti-inflammatory and antibacterial properties to promote wound healing, offering a multifaceted and effective approach to alleviating and managing the development of OM.[24–29] Additionally, we have successfully developed a semi-interpenetrating polymer network (semi-IPN) hydrogel, in which ε-Polylysine (PLL) as the framework offers unique features such as special degradation characteristics under the action of salivary amylase, antibacterial properties, and well-mucosal tissue adhesiveness suitable for the oral environment. The encapsulation of DNase-I and ORI into semi-IPN hydrogel prolongs their retention time, thereby accelerating the oral wound healing process.[30] A major limitation to the therapeutic efficacy of ENs is their poor retention and instability in vivo.[31] Thus, the semi-IPN hydrogel serves as an ideal carrier for ENs, and the encapsulation of ENs in semi-IPN hydrogel can be utilized as a long-term preservation strategy for ENs. The ORI/ENs will be incorporated into the semi-IPN hydrogel (ORI/ENs/Gel) for targeted delivery and controlled release of the drug in the oral cavity.

In this study, ENs were extracted from the regionally characteristic medicinal plant, *Rabdosia rubescens* in Henan Province, and then the ENs were loaded with homologous drug ORI using a physical squeezing method to construct biomimetic drug-loaded nanovesicles. Following characterization, ORI/ENs were combined with a biocompatible semi-IPN hydrogel (ORI/ENs/Gel) to develop a novel dressing for chemoradiotherapy-induced OM. The biocompatibility and antibacterial properties of ORI/ENs/Gel were observed in vitro. The therapeutic effect of ORI/ENs/Gel on OM wound healing was assessed and the potential mechanisms were further probed in vivo.

Materials and Methods

Materials, Cell Lines, and Animals

ORI, maleic anhydride, and hydroxyethyl starch (HES) were purchased from Shanghai Aladdin Reagent Co., Ltd., China. Maleic anhydride (MA), PLL, and N,N-dimethylformamide (DMF) were provided by Tianjin Kemiou Chemical Reagent Co., Ltd., China. Fresh leaves of *Rabdosia rubescens* were sourced in April 2023 from the Wangwu Mountain *Rabdosia rubescens* planting base in Jiyuan, Henan Province, China. The sample was identified by Prof. Jieli Lv from School of Pharmacy, Xinxiang Medical University. A voucher specimen (2023-S0428) was deposited with the Herbarium of School of Life Science and Technology, Xinxiang Medical University.

Mouse Fibroblast (L929) Cells were obtained from the Cold Spring Biotech Corp Company and incubated in DMEM medium (Solarbio Science & Technology, Beijing, China) supplemented with 1% penicillin-streptomycin as well as 10% FBS (BI Biological Industries, Israel) at 37°C in an environment of 5% CO_2.

All animal experiments were approved by the Ethics Committee Animal Experiments of Xinxiang Medical University (No. 202202488) and were performed in accordance with the Xinxiang Medical University guidelines for the welfare and ethics of experimental animals. SPF adult KM mice (20–24 g) and SD rats (200–250 g) were purchased from Henan Xincheng Youkang Biotechnology Co., Ltd. (Zhengzhou, China) and were housed at a temperature of 22–24°C with a 12 h light-dark cycle. Our study provided autoclaved water and a rodent diet (Huanyu Biotechnology Co., Ltd., Beijing, China) for the animals with ad libitum access.

Isolation and Purification of Rabdosia rubescens-Derived ENs

Fresh *Rabdosia rubescens* leaves were carefully washed with DI water and broken with prechilled PBS to extract the supernatant. After three minutes of mixing using a crusher, the mixture was centrifuged with a gradient of 5000 g for

30 min, 8000 g for 45 min, and 2 times at 10,000 g for 1 h to remove unbroken tissue pieces and obtain the supernatant. To remove larger particles, the supernatant was further centrifuged at 50,000 g for 1 h. The supernatant after initial purification was then subjected to ultra-centrifugation at 150,000 g for 90 min to collect the pellets containing the exosomes. To further access purified exosomes, the pellets were re-suspended with 3 mL of PBS and collected using a 0.45 μm filter membrane. All work was performed on ice and *Rabdosia rubescens*-derived exosomes (ENs) were stored at −80°C until analysis.

Characterization of ENs

The ENs were added to copper grids and negatively dyed with 0.75% uranyl formate for TEM observation to obtain the morphology and size. Dynamic light scattering (90 Plus Particles Size Analyzer, Malvern nanoZS, England) was performed to assess the mean particle size and size distribution. The morphology and size of ORI/ENs were characterized by the same methodology. The total lipid content of ENs was extracted using the Bligh and Dyer method.[32] ENs were mixed with an equal volume of chloroform/methanol (v/v, 2:1) solution, and the organic phase was collected and dried to obtain purified lipid samples. These samples were then weighed to calculate the lipid content. The total protein content of ENs was extracted using RIPA lysis buffer and quantified with a BCA protein kit (Absin Biotechnology Co., Ltd., Shanghai, China). Then, the proteins (30 μg in each lane) were subjected to SDS-PAGE separation (Servicebio, Wuhan, China) and visualized using BeyoBlue™ super-fast Coomassie Blue staining solution (Beyotime Biotechnology Co., Ltd., Shanghai, China) to obtain the protein band distribution. Isolation of RNA from ENs was performed using BRIzol™ universal total RNA isolation reagent (BIOEAST Biotechnology Co., Ltd., Hangzhou, China) and was further purified using the PrimeScript™ RT reagent kit (TaKaRa, Tokyo, Japan). A UV spectrophotometer was then employed to monitor the RNA levels. The purified RNA was treated with or without RNase A (Beyotime Biotechnology Co., Ltd., Shanghai, China) and subsequently separated on a 1.5% agarose gel. A 0.1–10 kbp RNA ladder was used as a size marker.

Preparation of ORI/ENs/Gel

We synthesized binary copolymers (PMD) of maleic anhydride and dimethyl acrylamide through a radical polymerization reaction. Subsequently, semi-IPN hydrogel were prepared via an amino-anhydride reaction in water, as previously reported.[30,33] The ENs (1 mg/mL) were mixed with the drug ORI (2 mg/mL) using a physical extrusion method, and the mixture was then repeatedly passed through the nanoporous membrane to obtain drug-loaded nanovesicles ORI/ENs. PMD (0.2025 g), HES (0.05 g), and PLL (0.0283 g) were added into ENs/ORI solution (1 mL) and stirred. Subsequently, the drug-loaded semi-interpenetrating network hydrogel (ORI/ENs/Gel) was rapidly obtained by titrating the pH to 8.0 at 37°C. In addition, semi-IPN hydrogel with ORI, ENs, and ORI+ENs was also prepared following the above method and named ORI/Gel, ENs/Gel, and ORI+ENs/Gel, respectively.

Characterization of ORI/ENs/Gel

SEM

A ZEISS Sigma 300 field emission SEM (Xplore, Oxford) was utilized to assess the morphology of ORI/ENs/Gel. The lyophilized samples were subjected to gold sputtering, and the morphology images were captured at an accelerating voltage of 3 kV.

Release Analysis of ORI/ENs/Gel

The drug loading content (LC) and encapsulation efficiency (EE) of ORI in ORI/ENs were evaluated. A controlled amount of ORI/ENs was formulated in PBS and the ORI content was subsequently analyzed using HPLC. The detection wavelength for ORI was set at 239 nm with a UV detector (G4212B Agilent, Germany). A Daisogel C18-10u-120Å, ID20 mm x 150 mm, 5 μm column equipped with a C18 preparative column was selected for UV detection. The mobile phase was constituted by water to methanol (48:52, v/v) and the column temperature was maintained at 25°C. ENs without any drug were considered as blanks. The following formula (1) and (2) were used to estimate the LC and EE of ORI:

LC = (Weight of ORI enclosed within ENs / Weight of ENs) × 100% (1)

EE = (ORI charged in ENs / overall weight of ORI) × 100% (2)

The in vitro release of ORI was also evaluated by the HPLC method. The in vitro release of ORI was also evaluated using the HPLC method. The ORI/Gel and ORI/ENs/Gel were incubated in 2 mL of PBS supplemented with 60 U/mL of α-amylase. At each collection point, a volume of PBS was removed and centrifuged at 4000 rpm for up to 5 min, after which it was replenished with an equal volume of fresh PBS. The centrifuged solution was then analyzed to determine the content of ORI released as described above.

In vitro Biological Properties

In vitro Cytotoxicity Assay MTT

The in vitro cytotoxicity of ENs/Gel, ORI/Gel, ORI+ENs/Gel, and ORI/ENs/Gel was evaluated in L929 cells using the MTT assay. Briefly, ENs/Gel, ORI/Gel, ORI+ENs/Gel, and ORI/ENs/Gel were extracted with PBS for 48 h at 37°C to obtain the leachates. When the confluence of L929 cells in each well reached about 75–85% in 96-well plates, the leachates at concentrations of 1, 10, and 100 μg/mL were added. After 48 h of co-incubation, MTT was introduced to the cells. The OD value of the blue-purple formazan formed was detected at 490 nm by applying an enzyme labeling detection instrument (Multiskan® GO, Thermo Fisher Scientific, MA, USA).

Scratch Assay

Cells were inoculated into 24-well plates and allowed to form monolayers with a density close to 80%. The cell was scratched linearly using a pipette tip of 200 μL to mimic an incision wound after 24 h of starvation in a medium without FBS. The cells were rinsed to eliminate cell debris, and incubated in a medium containing 1% FBS at 37°C. Besides, the medium was supplemented with PBS and the leachates of ENs/Gel, ORI/Gel, ORI+ENs/Gel, and ORI/ENs/Gel. At desired time intervals (24, 48, and 72 h), cells were photographed and the width of the scratch was measured using Image J software. The rate of cell migration was calculated following the formula (3) below:

Migration Area Rate (%) = ((A0 − A1)/A0) × 100% (3)

A0: initial scratch areas; A1: final scratch areas after treatment.

Hemolysis Assay

Fresh blood obtained from the eyeballs of mice was utilized for the hemolysis test. Mouse blood mixed with pre-cooled saline was centrifuged using a cryogenic centrifuge at 1500 rpm for 10 min. The supernatant was then aspirated and washed three times with PBS, until it became clear and colorless. 200 μL centrifuged erythrocytes and 800 μL ORI/ENs/Gel leachates at concentrations of 10, 20, 40, 60, and 80 mg/mL were co-incubated for 4 h at 37°C. The leachates were replaced with ultrapure water and saline solution, which served as the positive and negative controls, respectively. The mixture solutions were subsequently centrifuged at 12,000 rpm for 5 min, and the OD value was measured at 540 nm to access the hemolysis. Hemolysis is caused by the leakage of hemoglobin from lysed red blood cells, and the hemolysis ratio (%) was estimated as follows:

Hemolysis Ratio (%) = $(OD_{Sample} - OD_{Negative\ Control})/(OD_{Positive\ Control} - OD_{Blank}) \times 100\%$.

Vitro Antibacterial Assay

All materials were sterilized using UV irradiation for 30 min prior to use. To study the antibacterial properties of the composite hydrogel systems, *Escherichia coli* (*E. coli*, ATCC 25922) and *Staphylococcus aureus* (*S. aureus*, ATCC 29213) were chosen to establish bacterial models. The strains were initially revived rapidly to obtain a bacterial suspension. The test groups were divided into five groups: control, ENs/Gel, ORI/Gel, ORI+ENs/Gel, and ORI/ENs/Gel. The bacterial suspension (10^4–10^5 CFU/mL) was incubated with the different groups for 12 h, after which the supernatant was collected and spread onto plates, which were further culture for 3 h or 6 h at 37°C. Subsequently, the individual colonies on the plates were photographed, and the results were recorded for comparison. Negative controls were also set up without any hydrogel. To count the colonies in each group, three replicate experiments were performed. The antibacterial efficacy (inhibition ratio) for each group at each time point was assessed as follows:

Inhibition Ratio (%) = ($N_{Control}$ - N_{Sample})/$N_{Control}$ × 100%. $N_{Control}$: the number of colonies in the control group, N_{Sample}: the number of colonies in the treatment groups.

Acute Toxicity Test in vivo

The acute toxicity of ORI/ENs/Gel was evaluated in vivo according to a previously reported method.[34] Fifteen male and fifteen female KM mice (20–25 g) were utilized for perform the acute toxicity assessment of ORI/ENs/Gel. The thirty mice were randomly divided into experimental and control groups, namely the ENs/Gel, ORI/Gel, ORI+ENs/Gel, ORI/ENs/Gel, and control groups, with each group containing an equal number of males and females. Mice in the experimental groups were administered the leachates of ENs/Gel, ORI/Gel, ORI+ENs/Gel, and ORI/ENs/Gel via the tail vein at the predetermined time points (the 1st day and 3rd days), while the control group received an equivalent dose of PBS. Body weight (BW) and food intake were observed every two days. The mice were sacrificed, and their major organs (heart, liver, spleen, lung, kidney, and tongue) were collected and preserved in 4% paraformaldehyde for further histopathological examination after 14 days of observation. In addition, blood samples were collected for hematological and biochemical analyses using a hematology analyzer (BC-7500CRP, Mindray Automated Hematology Analyzer) and a biochemical analyzer (AU5800, Beckman Coulter Chemistry Analyzer).

In vivo Wound Healing Effect

After one week of adaptive feeding, Irritation (X-ray irradiator, X-Rad 225XL, total RT Dose 200cy, 1min) was performed on the first day (−1d), and Paclitaxel (APEXBIO, Jiangsu, China) was administered intraperitoneally at a dose of 60 mg/kg on the following day (0d) to the rats. Subsequently, 25% acetic acid was applied topically to the lower lip to induce ulcer formation (0d). Afterward, the rats were randomly arranged into five groups (n=12/group): control, ENs/IPN, ORI/IPN, ORI+ENs/IPN, and ORI/ENs/IPN groups.

After the successful establishment of the chemoradiotherapy-induced oral mucositis (OM) model, treatment was initiated on the 3rd day (1d). Treatments for the ENs/Gel, ORI/Gel, ORI+ENs/Gel, and ORI/ENs/Gel groups were administered every 24 h. Wound images of the different groups were captured on Days 2, 4, 6, 8, 10, and 12. Additionally, the food intake and body weight were monitored and recorded every other day.

Histological Analysis of Oral Mucosal Tissues

On the final day of treatment, all rats were sacrificed. Subsequently, the oral mucosal wound samples were cut out, and preserved in 4% paraformaldehyde for further staining and analysis. Hematoxylin and eosin (H&E), and Masson's trichrome staining were employed to assess wound regeneration and collagen formation. Histological analysis was carried out on the major organs of the rats using H&E staining exclusively.

Cytokine Contents in the Oral Mucosal Tissue

Fresh oral mucosal samples (100 mg) were collected and homogenized in PBS. Then, the supernatants were obtained by centrifugation at 12,000 g and 4°C for 15 min, and the protein quantification was performed using the BCA protein kit (Absin Biotechnology Co., Ltd., Shanghai, China). As recommended by the manufacturers of IL-1β, IL-6, and TNF-α ELISA kits (QuantiCyto® No: ERC003, NEOBIOSCIENCE CO., Ltd)., the concentrations of IL-1β, IL-6, and TNF-α were tested and recorded in units of pg/L.

Western Blot

Oral mucosal tissues were fragmented using RIPA lysis buffer through ultrasonication to obtain homogenates. Following centrifugation of the homogenates at 12,000 g and 4°C for 15 min, the supernatants were extracted and analyzed for protein content using BCA protein kit (Absin Biotechnology Co., Ltd., Shanghai, China). The proteins (24 μg in each lane) were subjected to SDS-PAGE separation (Servicebio, Wuhan, China) and diverted to PVDF membrane (Epizyme Biotech, Shanghai, China), after which they were conjugated with specific primary antibodies and horseradish peroxidase-conjugated secondary anti-rabbit or anti-mouse antibodies. Protein images were captured using the CLINX ECL

Gel Imaging System (CLINX Scientific Instruments Co., Shanghai, China). Relative quantitative analysis of the protein bands was performed using Image J software (National Institutes of Health, USA).

Statistical Analysis

Data are represented as mean ± SD and all statistical analyses were performed with GraphPad Prism 9.0. Student's *t*-test and post hoc Tukey's tests were assessed for significance analyses. P values less than 0.05 were considered statistically significant.

Results and Discussions

Preparation and Characterization of ENs and ORI/ENs

ENs were purified from *Rabdosia rubescens* by sequential ultra-centrifugations (Figure 1A). Transmission electron microscopy (TEM) was used to characterize the morphologies of ENs. ENs revealed lipid bilayer membrane structure and cell-like circular morphology (Figure 1B). The particle size distributions of ENs and ORI/ENs were measured using dynamic light scattering. The average diameter of ENs were 151.4 ± 29.2 nm (Figure 1C). Components within ENs were further investigated. The molecular weights of the proteins in ENs were between 10–200 kDa, indicating presence of a wide range of proteins with biological activity (Figure 1D). The nucleic acids in ENs were predominantly small RNA, as supported by the finding that RNase A treatment resulted in utter degradation of the nucleic acids (Figure 1E). The concentrations of proteins, nucleic acids, and lipids in ENs were determined to be 21.655 ± 4.85 mg/mL, 1.0342 ± 0.35 mg/mL and 16.9 ± 0.72 mg/mL, respectively (Figure 1F). Notably, these results established that the structure and

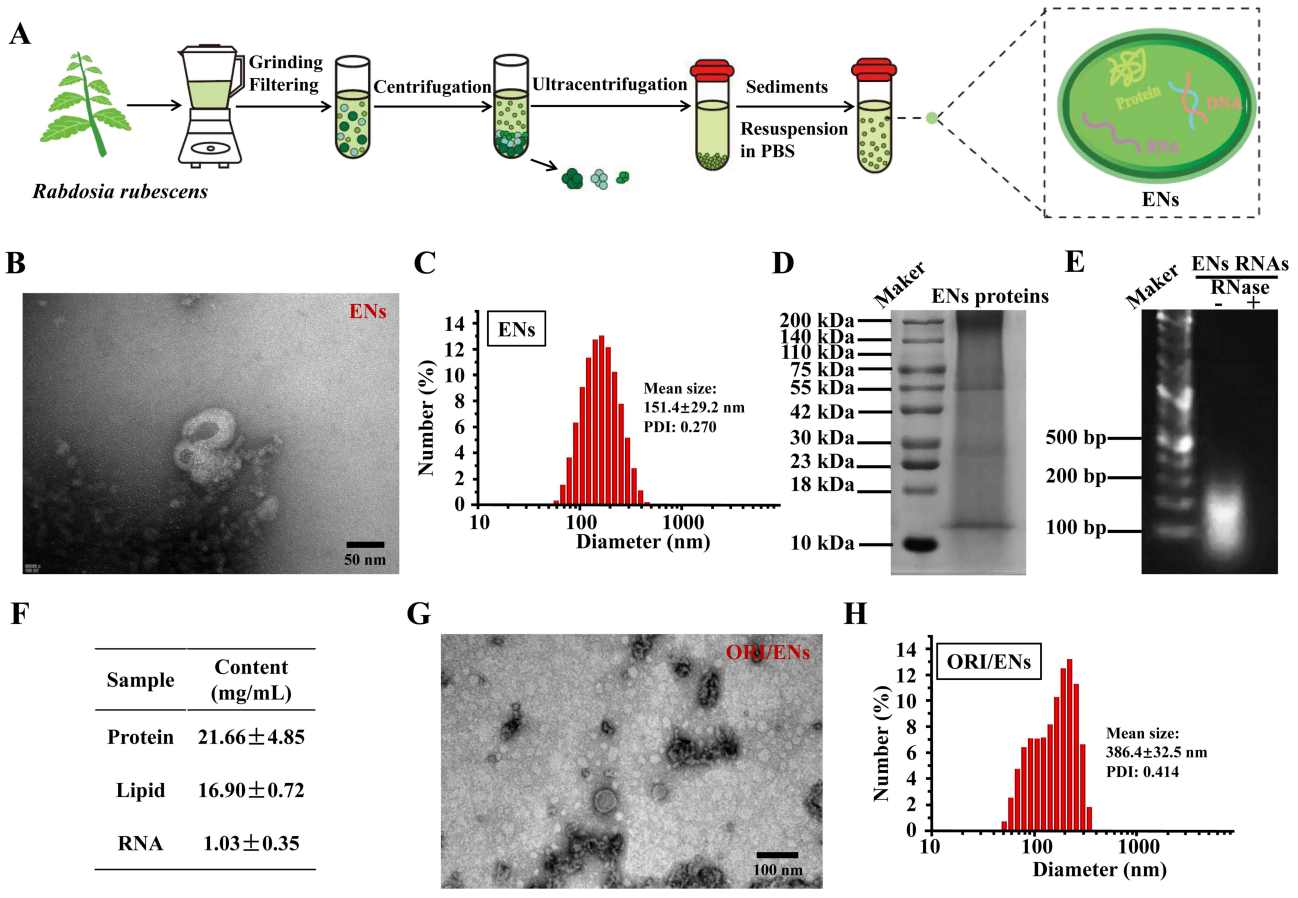

Sample	Content (mg/mL)
Protein	21.66±4.85
Lipid	16.90±0.72
RNA	1.03±0.35

Figure 1 Characterization of the ENs and ORI/ENs. (**A**) Schematic illustration of the extraction process of ENs. (**B**) TEM diagrams of ENs. (**C**) Particle size distribution of ENs. (**D**) Distribution of ENs protein bands. (**E**) Agarose gel analysis image of ENs RNA. (**F**) The protein, lipid, and RNA contents of ENs. (**G**) SEM observation of ORI/ENs. (**H**) Particle size distribution of ORI/ENs.

https://doi.org/10.2147/IJN.S508530

composition of ENs are similar to mammal-derived exosomes (MDEs), which contain RNA, proteins, and lipids that regulate physiological processes and exert therapeutic effects, such as antibacterial and anti-inflammatory properties.[35–37]

Consistent with the results observed in ENs, the lipid bilayer features of ORI/ENs were also visible and the particle size of ORI/ENs was increased to 381.4 ± 32.5 nm, indicating successful drug encapsulation without compromising the bilayer structure of ENs (Figure 1G-H). Moreover, we analyzed the LC and EE of ORI in ORI/ENs. The EE and LC of ORI in ORI/ENs were 76.4 ± 3.2% and 9.21 ± 0.45%, respectively, suggesting that ENs exhibited a high loading efficiency for the homologous drug ORI. These results revealed that ORI/ENs were proved to have the characteristic structure and functionality of extracellular vesicles.

Characterization and Biocompatibility of ORI/ENs Released from Semi-IPN Hydrogel

We integrated ORI/ENs into the semi-IPN hydrogel with the aim of significantly extending their retention time at the wound sites (Figure 2A). The three-dimensional mesh structure of ORI/ENs/Gel was observed using SEM and circular protrusions with regular morphology were observed in interconnected porous structures with pore diameters larger than 100 μm, which indicated that ORI/ENs was uniformly distributed in semi-IPN hydrogel (Figure 2B). Subsequently, the release profiles of ORI from semi-IPN hydrogel and ORI/ENs/Gel were evaluated. In the case of ORI/Gel, ORI were rapidly released, reaching its peak concentration at 3.5 h. In contrast, in the ORI/ENs/Gel group, the release of ORI was sustained, remaining stable until 7 h, indicating a longer drug release duration (Figure 2C). This result indicated that ORI/ENs/Gel has a more prolonged drug release time compared to the semi-IPN hydrogel, which can be attributed to the extended retention time of ENs. longer drug release time than pure semi-IPN hydrogel, which was dependent on the prolonged the retention time of ENs. In addition, the morphology of ORI/ENs released from the semi-IPN hydrogel was similar to that of the free ENs (Figure 2D). Therefore, the semi-IPN hydrogel, acting as a carrier, not only preserved the integrity of ENs but also facilitated the sustained release of ORI/ENs, thus promoting effective drug delivery to the wound site.

Furthermore, the application of the ORI/ENs/Gel to the mucosa would lead to their contact with blood. A desirable wound dressing should display minimal or no hemolysis when in touch with a bleeding wound site.[38] The in vitro hemolysis assay was carried out to assess the hemocompatibility of ORI/ENs/Gel at different concentrations. As shown in Figure 2E, the supernatants from all tested concentrations of ORI/ENs/Gel exhibited transparency, with precipitated erythrocytes at the bottom, resembling the negative PBS group. In turn, the positive deionized water group completely dissolved and produced a red color. The hemolysis ratio of ORI/ENs/Gel at different concentrations (10–-100 μg/mL) was less than 2%, even at the highest concentration. Hence, these results confirmed that the biocompatibility of ORI/ENs/Gel with the blood contributed to the preservation of their bioactivity, enabling it to be applied as oral wound repair materials.

It is well known that the key factor allowed biomaterials enabling the use of dressings in direct contact with wounds is due to its low cytotoxicity.[39] In addition, it has been shown that decreased or impaired cell migration ability prevented wound healing and predisposed to localized scar formation, which might affect regeneration outcomes and prolong the healing time.[39] To verify whether ORI/ENs/Gel affected cell activity, proliferation and migration capacity, thereby delaying growth and wound healing, we performed MTT and scratch assay, respectively. When co-incubated with L929 cells for 48 h at different concentrations (0–100 μg/mL), the cell viability of ENs/Gel, ORI/Gel, ORI+ENs/Gel, and ORI/ENs/Gel maintained above 85%, indicating that ORI/ENs/Gel have no significant cytotoxicity (Figure 2F). Following the scratch assay, cell migration was recorded at 0, 24, 48, and 72 h. Notably, compared with the control group, there was no significant difference in the cell gap of ENs/Gel, ORI/Gel, ORI+ENs/Gel groups, whereas the cell gap was narrower after ORI/ENs/Gel treatment at 72 h (Figure 2G). Additionally, the ORI/ENs/Gel group acquired a larger migratory area than the ENs/Gel group at both 24 and 48 h. It was significantly larger than that of the ORI/Gel group only at 48 h (Figure 2H). Overall, ORI/ENs/Gel enhanced the migratory ability of L929 cells. These finding indicated that ORI/ENs/Gel were biocompatible and performed best.

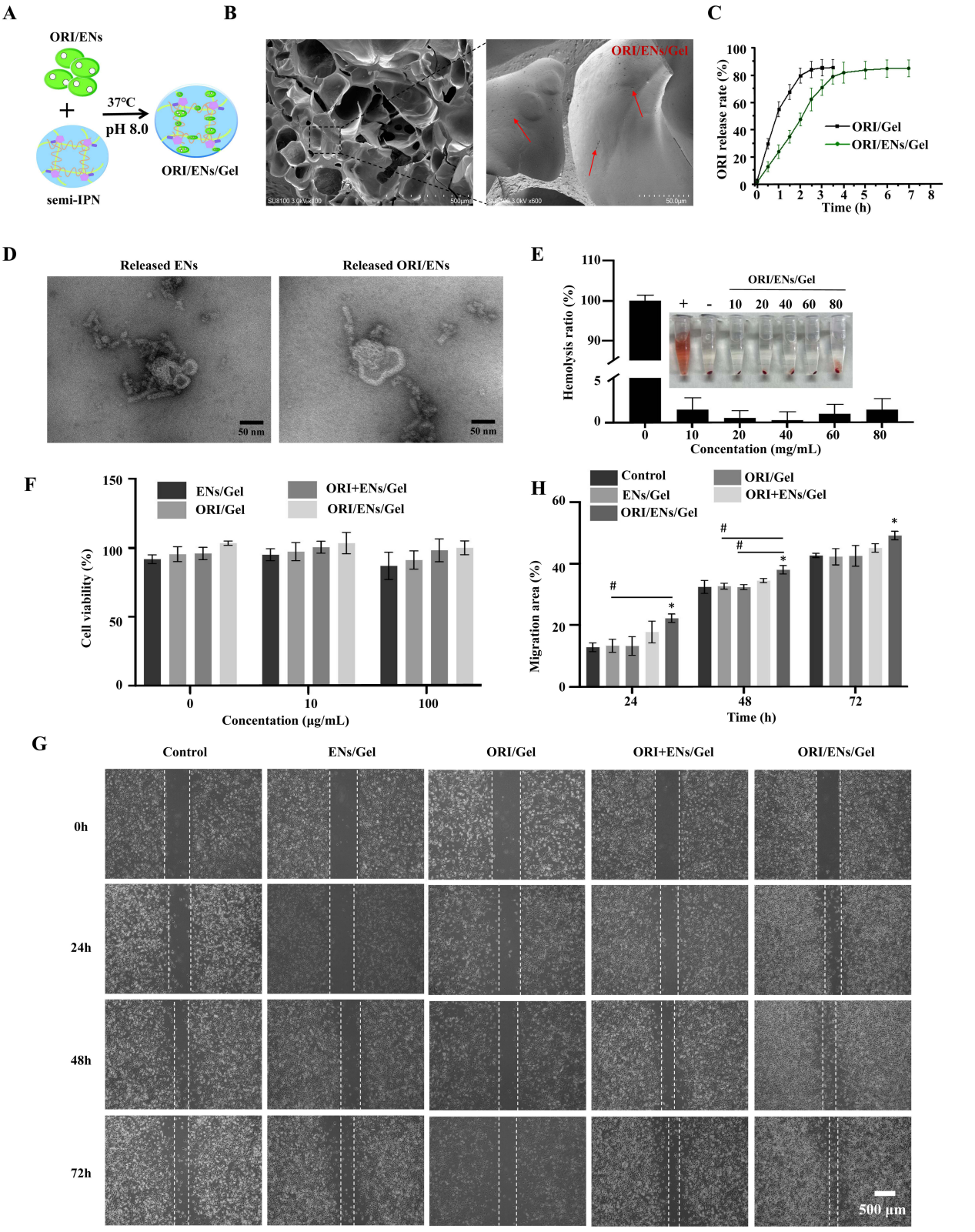

Figure 2 Characterization and biocompatibility of ORI/ENs loaded into semi-IPN hydrogel. (**A**) Schematic diagram depicting the preparation process of ORI/ENs/Gel. (**B**) The SEM images of ORI/ENs/Gel. (**C**) ORI release profiles from IPN and ORI/ENs/Gel. (**D**) The TEM images of ENs and ORI/ENs released from semi-IPN hydrogel. (**E**) Hemolysis test under different concentrations of ORI/ENs/Gel. (**F**) Effect of ORI/ENs/Gel on the cell viability of L929 cells. (**G**) Assessment of L929 cells proliferation and migration capacity. (**H**) Relative quantitative analysis of cell gap closure. *$p < 0.05$, vs the control group; #$p < 0.05$, vs ORI/ENs/Gel group, n=3.

https://doi.org/10.2147/IJN.S508530

The Antibacterial Activity in vitro of ORI/ENs/Gel

It has been reported that the oral environment is humid and oral wounds secrete large amounts of exudate, offering an optimal environment for bacterial proliferation. This condition is exacerbated in infected oral wounds, which can develop into chronic refractory wounds. Notably, infection is thought to be the most common cause of delayed OM healing.[40–43] Thus, it is crucial that biomaterials used for infected and refractory oral wound treatment have antibacterial activity. We evaluated the antibacterial activity of ENs/Gel, ORI/Gel, ORI+ENs/Gel, and ORI/ENs/Gel against two prevalent wound bacteria (*S. aureus* and *E. coli*) against the blank group.[6,44] It can be seen that bacteria in the control group grew well and the bacterial count has reached 90%. Figure 3A and C indicate that after 3 h and 6 h of direct contact with bacteria, the growth of *S. aureus* was significantly reduced in ENs/Gel, ORI/Gel, ORI+ENs/Gel, and ORI/ENs/Gel groups, while the antibacterial effect on *E. coli* was slight in the ENs/Gel group and higher in the ORI/Gel, ORI+ENs/Gel, and ORI/ENs/Gel groups. The inhibition of the proliferation of both bacteria in all groups had a time effect; prolonging the incubation time enhanced the inhibition effect. However, it is worth noting that ORI/ENs/Gel shows approximately 100% inhibition ratio against both bacterial strains and exhibited significantly higher antibacterial activity compared to ORI+ENs/Gel (Figure 3B and D). These results were consistent with the characterization of ORI release, and they demonstrated that the antibacterial effect of ORI/ENs/Gel was highest due to the slow release and synergistic properties of encapsulating ORI in ENs.

Acute Toxicity Test in vivo

In in vitro studies, we observed no significant toxicity of ORI/ENs loaded in semi-IPN hydrogel to L929 cells. To further verify the biosafety of hydrogel in vivo, the leachates of ENs/Gel, ORI/Gel, ORI+ENs/Gel, and ORI/ENs/Gel at the dose of 100 mg/kg body weight were injected via *i.v.* to the mice, and there were neither adverse effects nor mortality, compared to the control group (PBS). As shown in Figure 4A, H and E staining revealed no obvious morphological lesion was observed in the heart, liver, spleen, lung, tongue, and kidney of the treatment groups compared to the control group. Simultaneously, we tracked the changes in food intake and body weight in the treated and control groups

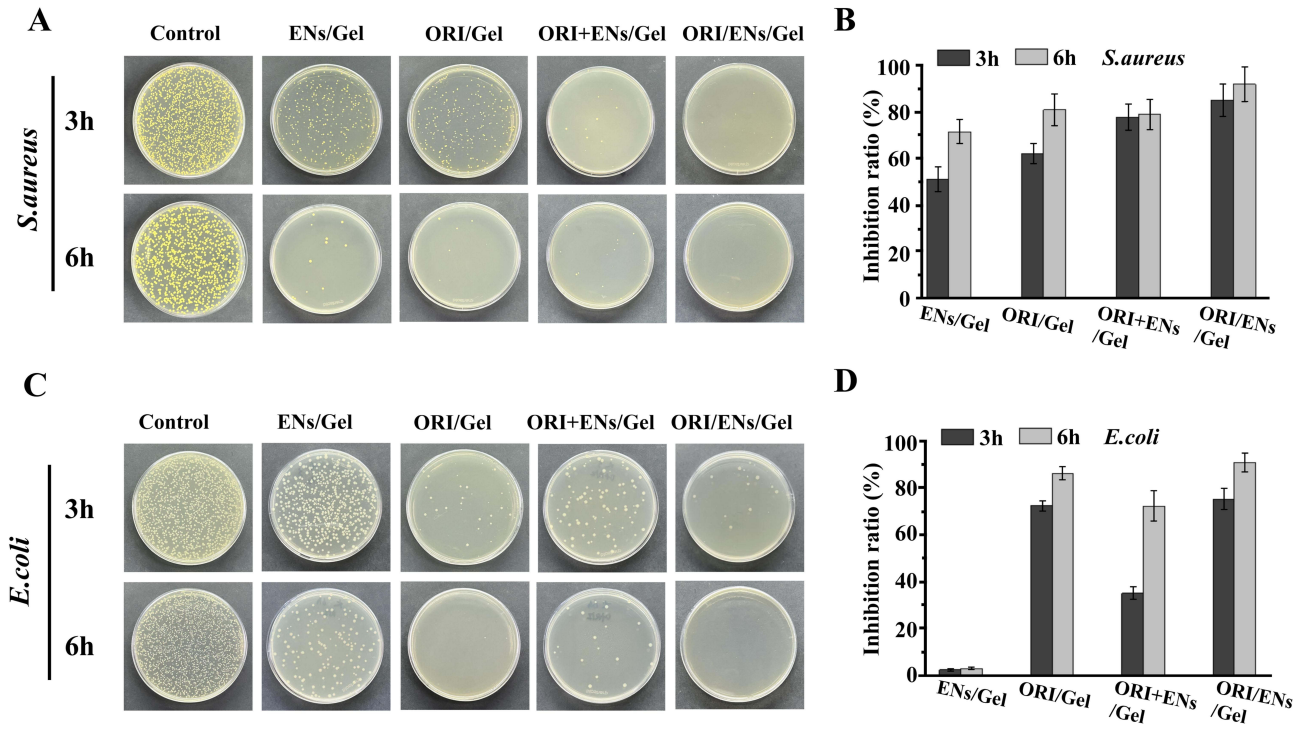

Figure 3 Antibacterial ability of ORI/ENs/Gel. (**A**) Images of *S. aureus* colonies after incubation with control, ENs/Gel, ORI/Gel, ORI+ENs/Gel, and ORI/ENs/Gel in vitro. (**B**) Relative quantitative analysis of inhibition rate for *S. aureus*. (**C**) Images of *E. coli* colonies after incubation with control, ENs/Gel, ORI/Gel, ORI+ENs/Gel, and ORI/ENs/Gel in vitro. (**D**) Relative quantitative analysis of inhibition rate for *E. coli*.

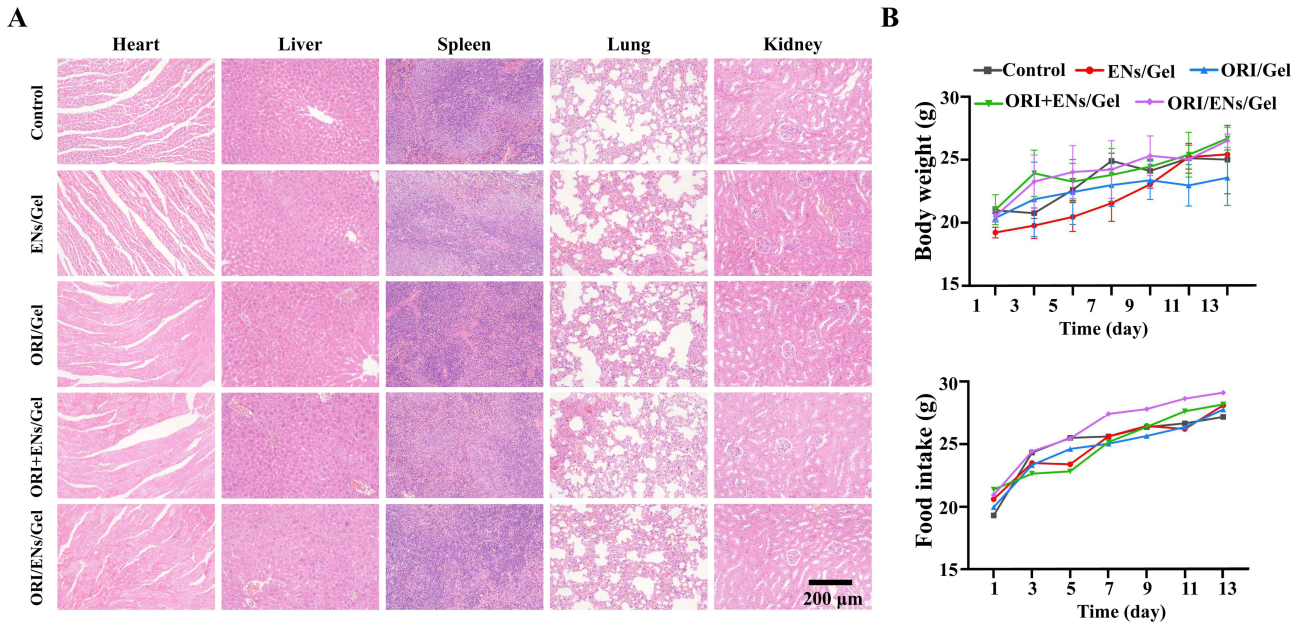

Figure 4 In vivo biocompatibility of ORI/ENs/Gel. (**A**) H&E staining of major organs. (**B**) Effect of the control, ENs/Gel, ORI/Gel, ORI+ENs/Gel, and ORI/ENs/Gel on the body weight and food intake.

(Figure 4B). The results evinced that there was no discernible discrepancy between the treatment and control groups in body weight and food intake. The data of hematological indexes (RBC, WBC, Neu, and Platelet), liver function biochemical indexes (AST and ALT), and kidney function biochemical indexes (BUN and CRE) between the control and treatment groups showed no significant difference on the 14th day, indicating that ENs/Gel, ORI/Gel, ORI+ENs/Gel, and ORI/ENs/Gel did not cause liver and kidney damage, infections, hemostatic and procoagulant disorders (Table 1). Overall, the ORI/ENs/Gel showed no significant adverse effects on the major organs and did not induce any metabolic abnormalities, demonstrating that ORI/ENs had a potential for tissue repair.

Effect of ORI/ENs/Gel on OM Wound Healing

With the global increase in the prevalence of tumors, OM is a major side effect of chemotherapy and radiotherapy, and improving delayed wound healing in the oral mucosa caused by chemoradiotherapy is of great importance.[45–47] In addition, since ORI/ENs/Gel had excellent bioactivities in vitro and ORI could be sustainably released from ORI/ENs/Gel as demonstrated above, we next evaluated the tissue regenerative capacity of ENs/Gel, ORI/Gel, ORI+ENs/Gel, and

Table 1 Hematological and Biochemical Parameters of KM Mice Blood

	control	ENs/Gel	ORI/Gel	ORI+ ENs/Gel	ORI/ENs/Gel
RBC ($\times 10^{12}$/L)	4.78±0.44	4.67±0.50	4.42±0.20	4.65±0.53	4.55±0.43
WBC ($\times 10^{9}$/L)	5.89±0.42	5.48±0.71	6.02±0.64	5.88±0.55	5.94±0.51
Neu ($\times 10^{9}$/L)	3.83±0.61	4.28±0.54	3.77±0.82	3.33±0.75	4.20±0.74
Platelet ($\times 10^{9}$/L)	307±75	247±123	221±111	207±102	289±101
ALT (U/L)	28±2	20±4	18±2	19±3	44±10
AST (U/L)	22±5	23±6	20±5	21±2	29±4
BUN (mmol/L)	3.53±1.20	6.71±1.32	3.98±1.41	5.54±1.45	4.24±1.15
Cr (μmol/L)	44±5	48±6	46±8	45±7	56±6

https://doi.org/10.2147/IJN.S508530

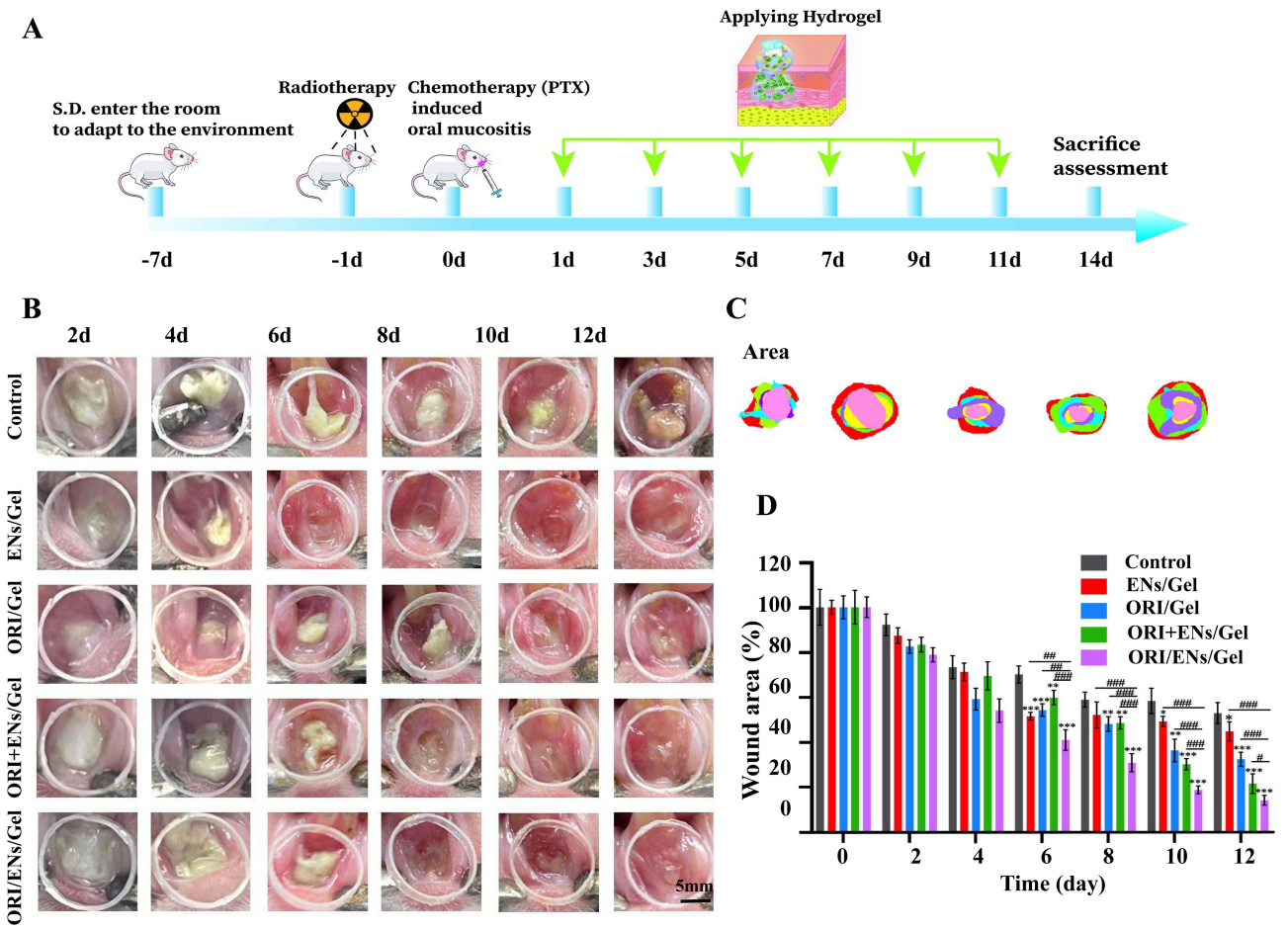

Figure 5 In vivo evaluation of ORI/ENs/Gel in the OM rats wound. (**A**) A scheme of chemoradiotherapy-induced OM modeling and hydrogel intervention. (**B**) Healing status of oral mucositis in control, ENs/Gel, ORI/Gel, ORI+ENs/Gel, and ORI/ENs/Gel. (**C**) Wound fractions healed by different treatments on days 2, 4, 6, 8, 10, and 12. (**D**) Quantitative analysis of oral mucosal wound area. *$p < 0.05$, **$p < 0.01$, ***$p < 0.001$, vs the control group; #$p < 0.05$, ##$p < 0.01$, ###$p < 0.001$, vs ORI/ENs/Gel group, n=3.

ORI/ENs/Gel in rat OM models. A rat model of OM was successfully constructed via chemoradiotherapy, and then the induced wounds were treated with the corresponding hydrogel (Figure 5A). As shown in Figure 5B-5C, representative images of OM wounds with different treatments were captured on days 2, 4, 6, 8, 10, and 12. The wound healing rate of the group treated with ORI/ENs/Gel was significantly faster, compared with ENs/Gel, ORI/Gel, ORI+ENs/Gel, and the control (treated by PBS) group at days 6, 8, 10, and 12. On the 12th day, the wounds of the ORI/ENs/Gel group were nearly recovered and presented a smooth surface. However, the other groups were still clearly visible, especially the control group. The results of the quantitative analysis were in line with the images presented in Figure 5D. To be more precise, on the 10th day, the wound area of the ORI/ENs/Gel group accounted for 18.9% ± 0.9%. By the 12th day, the wound areas of the control, ENs/Gel, ORI/Gel, and ORI + ENs/Gel groups remained at 52.9% ± 2.4%, 44.8 ± 2.1%, 32.7 ± 2.6%, and 21.6 ± 2.2%, respectively. In contrast, the wound area in the ORI/ENs/Gel group was only 14.2 ± 1.1%. The OM wound sites were treated with ENs/Gel, ORI/Gel, ORI+ENs/Gel, and ORI/ENs/Gel respectively. Remarkably, we discovered that ORI/ENs/Gel had the most rapid healing rate and the optimal healing outcome. These results strongly suggested that encapsulating ORI helped ENs promote OM wound healing, while further binding to semi-IPN hydrogel contributed to the performance of ORI/ENs in vivo. The ORI/ENs loaded in semi-IPN hydrogel retained biological activity, while the effects of ORI, ENs, and ORI+ENs were greatly weakened with the separation of ORI from ENs.

Patients with chemotherapy and/or radiotherapy-induced OM suffer from dysphagia due to wound pain and swelling, which may lead to dystrophy and reduce the effectiveness of treatment, along with the adverse effects of weight loss.[48,49] Thus, body weight and food intake were monitored to clarify the success of the chemoradiotherapy model and assess

drug therapeutic efficacy. ENs/Gel, ORI/Gel, ORI+ENs/Gel, and ORI/ENs/Gel groups exhibited a reversal of weight loss compared to the control group, especially the ORI/ENs/Gel group (Figure S1). Changes in intake parallel those in body weight, suggesting ORI/ENs/Gel might relieve pain and enhance oral comfort. Simultaneously, the in vivo histocompatibility and biosafety of the different treatment groups were further evaluated by H&E staining of major organs (heart, liver, spleen, lung, and kidney). The results indicated that no visible damage and pathological changes were observed in these major organs of the ENs/Gel, ORI/Gel, ORI+ENs/Gel, and ORI/ENs/Gel groups during the treatment, indicating that ORI/ENs/Gel had biological safety (Figure S2). Due to ulcer formation in the lower lip, the ORI/ENs/Gel came into contact with the tongue more frequently. Therefore, we conducted histopathological observations of the adjacent tongue tissue. The results showed no signs of inflammation or cell infiltration in any of the treatment groups. In general, the ORI/ENs/Gel exhibited biosafety and biocompatibility, indicating its potential to repair mucosal tissue.

ORI/ENs/Gel Facilitated Oral Wound Healing via Targeting NLRP3

It has been indicated that ORI possesses various biological properties, such as anti-inflammatory and antibacterial properties. In addition, NLRP3 was shown to be a target for ORI to mediate anti-inflammatory activity.[50] Previous studies have shown that the activation of NF-κB stimulates the expression of NLRP3, which promotes the secretion of pro-inflammatory factors such as IL-1β and TNF-α, consequently inducing an inflammatory response.[51–53] To clarify the role of ORI/ENs/Gel in the anti-inflammatory process, we tested the levels of pro-inflammatory cytokines, namely IL-6, TNF-α, and IL-1β in the wound area. The secretion of IL-6, IL-1β, and TNF-α was decreased by ENs/Gel, ORI/Gel, ORI +ENs/Gel, and ORI/ENs/Gel treatment, whereas ORI/ENs/Gel exhibited the lowest levels compared with those in other groups (Figure 6A-6C). We then analyzed the expression of NLRP3 and its upstream gene, both of which were associated with the NF-κB pathway, to probe the potential mechanism. Moreover, the Western blotting revealed that the expression of phosphorylated NF-κB (pNF-κB, p-P65) and IκBα (pIκBα), as well as NLRP3, was lower in ENs/Gel, ORI/Gel, ORI +ENs/Gel, and ORI/ENs/Gel groups than those in the control group (Figure 6D-6G). Notably, ORI/ENs/Gel displayed lower NLRP3 expression levels compared with ORI+ENs/Gel treatment, suggesting that ORI/ENs/Gel had a stronger inhibitory effect on the NLRP3 inflammasome and a more effective anti-inflammatory effect.

Wound healing is a complex biological process involving anti-inflammation, cell proliferation and migration, epithelialization, and extracellular matrix deposition.[54,55] To further observe the wound regeneration in detail, we examined the histological changes in the oral mucosal tissues (Figure 6H). The results of H&E staining showed the presence of granulation tissue, higher inflammatory cell infiltration, and disordered epidermal structures around the wound in the control group, indicating successful modeling. In contrast, the wounds treated with ENs/Gel, ORI/Gel, and ORI+ENs/Gel were partially repaired, exhibiting a reduction in inflammatory cell infiltration, wound closure, and epithelium regeneration. Among all the groups, the ORI/ENs/Gel displayed optimal wound healing with complete epithelial coverage. The collagen regeneration and deposition were essential to maintain tissue integrity and status, which is directly associated with wound healing.[56] Masson's trichrome staining of oral mucosal tissues was performed to assess the collagen production upon treatment. The collagen deposition was significantly higher in the ENs/Gel, ORI/Gel, ORI+ENs/Gel, and ORI/ENs/Gel groups than in the control group (Figure 6H). Moreover, the distribution and structure of collagen in the ORI/ENs/Gel group were thicker, tighter and more complete, which was superior to those in the other groups, indicating that the ORI/ENs/Gel had more collagen deposited on the wound surface. The re-epithelialization and collagen deposition revealed that the effectiveness of treatment with ENs was notably heightened following the encapsulation of ORI. The pro-inflammatory cytokines in the wound area were apparently decreased and the suppression of NLRP3 expression was more pronounced in the ORI/ENs/Gel group, which further demonstrated that ORI can be released and retained upon dual encapsulation of ENs and semi-IPN hydrogel, thus maintaining the inhibitory activity of NLRP3 to promote wound healing. It's also been proven that the addition of ORI in ENs synergistically enhances their biological activity.

Based on the above results, we found that with the sustained release from semi-IPN hydrogel, ORI/ENs specifically inhibited the expression of NLRP3 and further reduced the secretion of pro-inflammatory factors, which in turn promoted collagen deposition and re-epithelialization, thereby facilitating chemoradiotherapy-induced oral wound healing

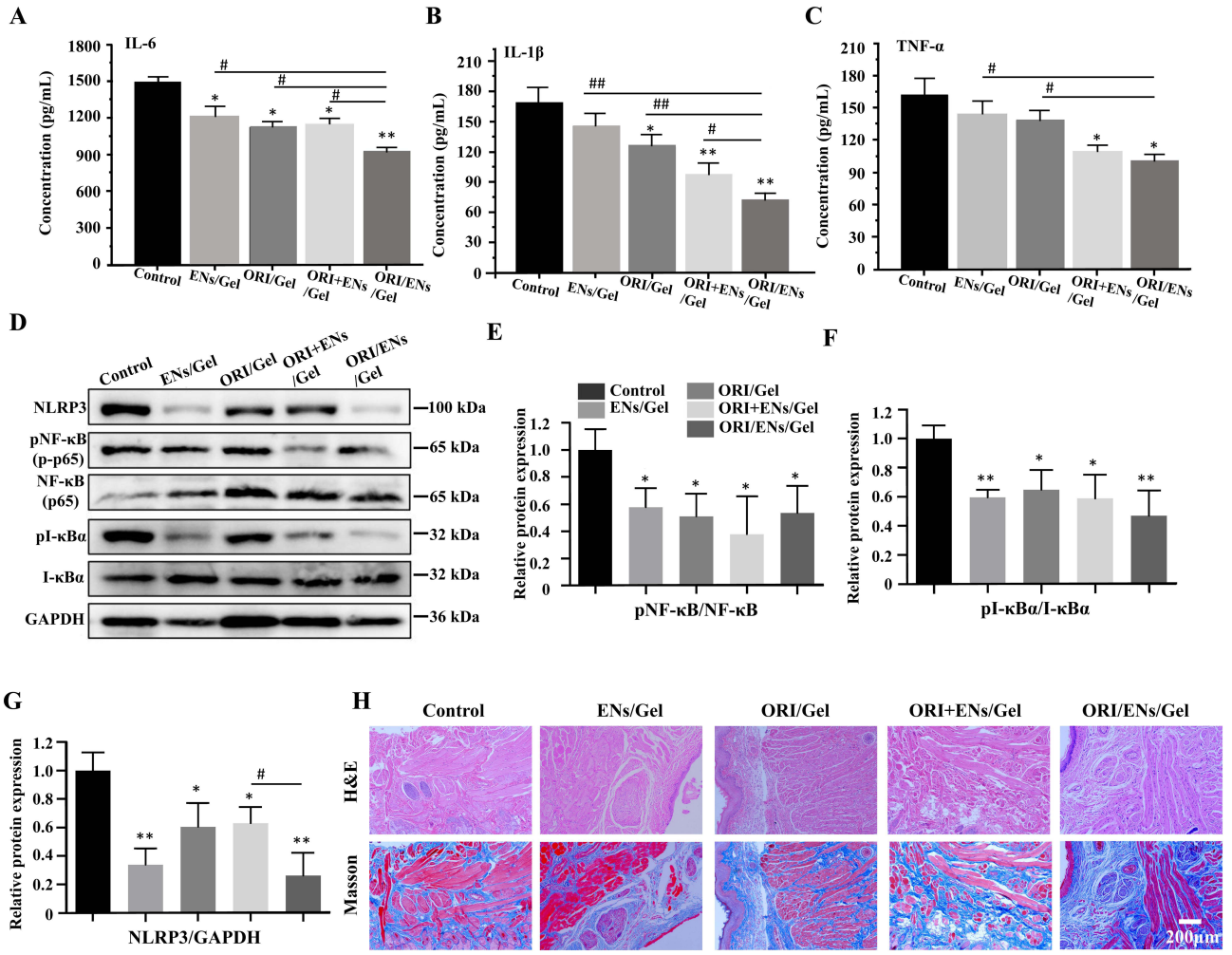

Figure 6 ORI/ENs/Gel promote wound healing by modulating the inflammatory response via the NF-κB/NLRP3 pathway. (**A**) The levels of IL-6. (**B**) The levels of IL-1β. (**C**) The levels of TNF-α. (**D**) Immunoblotting images of NLRP3, pNF-κB, NF-κB, pI-κB, I-κB, and GAPDH. (**E**) The protein expression level of pNF-κB relative to NF-κB. (**F**) The relative quantitative analysis of pI-κBα relative to I-κBα. (**G**) The relative quantitative analysis of NLRP3 relative to GAPDH. (**H**) (b) H&E staining and Masson staining of regenerated oral mucosal tissue in different groups at day 12. *p < 0.05, **p < 0.01, vs the control group; #p < 0.05, ##p < 0.01, vs ORI/ENs/Gel group, n=3.

(Figure 7). Hence, we considered that ORI/ENs/Gel exerted an anti-inflammatory effect mainly by targeting NLRP3 and exerting antibacterial effects, which contributed to the acceleration of wound healing in OM.

Conclusion

In conclusion, We developed a novel ORI/ENs/Gel hydrogel system for treating chemoradiotherapy-induced OM. The system was constructed by using ENs derived from a medicinal plant, *Rabdosia rubescens*, as the drug carrier for homologous drug ORI, which was also obtained from *Rabdosia rubescens*. The ORI/ENs were further incorporated into an IPN hydrogel. The ORI/ENs/Gel gradually dissolved in the presence of salivary amylase and released the ORI/ENs, which in turn penetrated and accumulated in the local microenvironment. The ORI was then released from the ENs and exhibited potent antibacterial and anti-inflammatory effects. Furthermore, the synergistic effects of the hydrogel and the co-loaded ENs/ORI effectively accelerated oral mucosal healing. This study contributes to the development of innovative strategies for improving the management of OM and other challenging wounds associated with chemoradiotherapy. Next, we plan to conduct future research using a tumor animal model in which OM is induced through combined radiation and chemotherapy treatments. This experimental approach will closely mimic the clinical scenarios encountered by cancer patients undergoing these therapies, enabling us to assess the efficacy and safety of the ORI/ENs/Gel hydrogel system in a more clinically relevant and realistic setting.

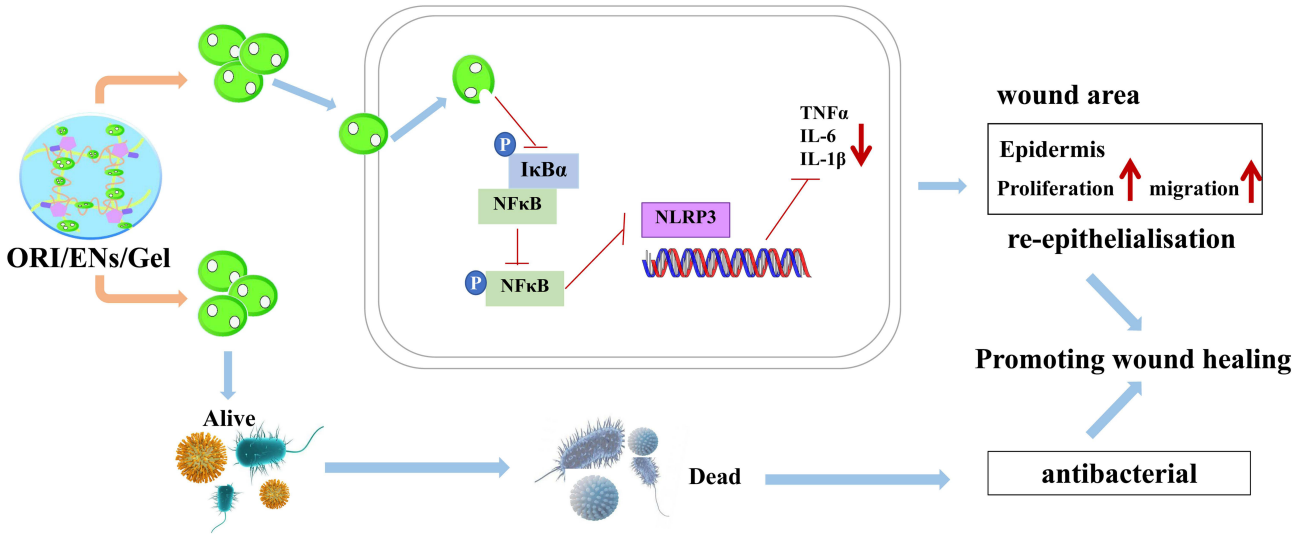

Figure 7 The potential mechanisms of ORI/ENs released from semi-IPN hydrogel to enhance oral wound healing via antibacterial and targeting NLRP3.

Abbreviations

OM, Oral mucositis; L929 cell, NCTC clone 929 [L cell, L-929, derivative of Strain L]; ENs, exosome-like nanovesicles; ORI, Oridonin; SEM, scanning electron microscope; TEM, transmission electron microscopy; PBS, dynamic light scattering; H&E, hematoxylin-eosin staining; semi-IPN hydrogel, semi-interpenetrating polymer network hydrogel; MTT, 3-(4,5-dimethylthiazol-2-yl)-2,5-diphenyltetrazolium bromide; CFU, colony-forming units; BCA, Bicinchoninic acid; SDS-PAGE, sodium dodecyl sulfate-polyacrylamide gel electrophoresis; PBS, phosphate buffer saline; pNF-κB, phosphorylated nuclear factor kappa-B; pIκBα, phosphorylated NF-κB inhibitor alpha; NLRP3, NOD-like receptor thermal protein domain associated protein 3; RBC, red blood cell; WBC, white blood cell; Neu, Neutrophil; BUN, blood urea nitrogen; Cr, creatinine; AST, aspartate transaminase; ALT, aspartate transaminase; IL-6, interleukin-6; IL-1β, interleukin-1beta; TNF-α, tumor necrosis factor-alpha.

Acknowledgments

This work was supported by the Key Technologies R&D Program of Henan Province (242102521008), the Key Scientific Research Projects of Colleges and Universities in Henan Province (24A320013), the Open Project Program of the Third Affiliated Hospital of Xinxiang Medical University (No. KFKTZD202102, KFKTYB202117), and the Graduate Research Innovation Support Project of Xinxiang Medical University (No. YJSCX202436Y, YJSCX202470Z).

Disclosure

The authors declare no conflicts of interest in this work.

References

1. Elad S, Yarom N, Zadik Y, et al. The broadening scope of oral mucositis and oral ulcerative mucosal toxicities of anticancer therapies. *CA Cancer J Clin*. 2022;72(1):57–77. doi:10.3322/caac.21704
2. Stoopler ET, Villa A, Bindakhil M, et al. Common Oral Conditions: a Review. *JAMA*. 2024;331(12):1045–1054. doi:10.1001/jama.2024.0953
3. Iovoli AJ, Turecki L, Qiu ML, et al. Severe Oral mucositis after intensity-modulated radiation therapy for head and neck cancer. *JAMA Network Open*. 2023;6(10):e2337265. doi:10.1001/jamanetworkopen.2023.37265
4. Elad S, Yarom N. The search for an effective therapy and pain relief for oral mucositis. *JAMA*. 2019;321(15):1459–1461. doi:10.1001/jama.2019.3269
5. Pulito C, Cristaudo A, Porta C, et al. Oral mucositis: the hidden side of cancer therapy. *J Exp Clin Cancer Res*. 2020;39(1):210. doi:10.1186/s13046-020-01715-7
6. Hong BY, Sobue T, Choquette L, et al. Chemotherapy-induced oral muco sitis is associated with detrimental bacterial dysbiosis. *Microbiome*. 2019;7(1):66. doi:10.1186/s40168-019-0679-5

7. Liu J, Zhang Z, Lin X, et al. Magnesium metal-organic framework microneedles loaded with curcumin for accelerating oral ulcer healing. *J Nanobiotech*. 2024;22(1):594. doi:10.1186/s12951-024-02873-y
8. Li Y, Zhu Z, Li S, et al. Exosomes: compositions, biogenesis, and mechanisms in diabetic wound healing. *J Nanobiotechnol*. 2024;22(1):398. doi:10.1186/s12951-024-02684-1
9. Kalluri R, LeBleu VS. The biology, function, and biomedical applications of exosomes. *Science*. 2020;367(6478):eaau6977. doi:10.1126/science.aau6977
10. Feng H, Yue Y, Zhang Y, et al. Plant-derived exosome-like nanoparticles: emerging nanosystems for enhanced tissue engineering. *Int J Nanomed*. 2024;19:1189–1204. doi:10.2147/IJN.S448905
11. Yi Q, Xu Z, Thakur A, et al. Current understanding of plant-derived exosome-like nanoparticles in regulating the inflammatory response and immune system microenvironment. *Pharmacol Res*. 2023;190:106733. doi:10.1016/j.phrs.2023.106733
12. Kim J, Li S, Zhang S, et al. Plant-derived exosome-like nanoparticles and their therapeutic activities. *Asian J Pharm Sci*. 2022;17(1):53–69. doi:10.1016/j.ajps.2021.05.006
13. Dai W, Dong Y, Han T, et al. Microenvironmental cue-regulated exosomes as therapeutic strategies for improving chronic wound healing. *NPG Asia Mater*. 2022;14(1):75. doi:10.1038/s41427-022-00419-y
14. Shen Z, Wang L, Xie X, et al. Sprayable, antimicrobial and immunoregulation hydrogel loading exosomes based on oxidized sodium alginate for efficient wound healing at skin graft donor sites and health detection. *Carbohydr Polym*. 2025;351:123098. doi:10.1016/j.carbpol.2024.123098
15. Han X, Saengow C, Ju L, et al. Exosome-coated oxygen nanobubble-laden hydrogel augments intracellular delivery of exosomes for enhanced wound healing. *Nat Commun*. 2024;15(1):3435. doi:10.1038/s41467-024-47696-5
16. Li W, Wu S, Ren L, et al. Development of an antiswelling hydrogel system incorporating M2-exosomes and photothermal effect for diabetic wound healing. *ACS Nano*. 2023;17(21):22106–22120. doi:10.1021/acsnano.3c09220
17. Xu Z, Dong M, Yin S, et al. Why traditional herbal medicine promotes wound healing: research from immune response, wound microbiome to controlled delivery. *Adv Drug Deliv Rev*. 2023;195:114764. doi:10.1016/j.addr.2023.114764
18. Zhou GB, Kang H, Wang L, et al. Oridonin, a diterpenoid extracted from medicinal herbs, targets AML1-ETO fusion protein and shows potent antitumor activity with low adverse effects on t(8;21) leukemia in vitro and in vivo. *Blood*. 2007;109(8):3441–3450. doi:10.1182/blood-2006-06-032250
19. He H, Jiang H, Chen Y, et al. Oridonin is a covalent NLRP3 inhibitor with strong anti-inflammasome activity. *Nat Commun*. 2018;9(1):2550. doi:10.1038/s41467-018-04947-6
20. Jia XM, Hao H, Zhang Q, et al. The bioavailability enhancement and insight into the action mechanism of poorly soluble natural compounds from co-crystals preparation: oridonin as an example. *Phytomedicine*. 2024;122:155179. doi:10.1016/j.phymed.2023.155179
21. Ding C, Zhang Y, Chen H, et al. Novel nitrogen-enriched oridonin analogues with thiazole-fused a-ring: protecting group-free synthesis, enhanced anticancer profile, and improved aqueous solubility. *J Med Chem*. 2013;56(12):5048–5058. doi:10.1021/jm400367n
22. Lv Y, Li W, Liao W, et al. Nano-drug delivery systems based on natural products. *Int J Nanomed*. 2024;19:541–569. doi:10.2147/IJN.S443692
23. Li M, Mao B, Tang X, et al. Lactic acid bacteria derived extracellular vesicles: emerging bioactive nanoparticles in modulating host health. *Gut Microbes*. 2024;16(1):2427311. doi:10.1080/19490976.2024.2427311
24. Fan MH, Zhang XZ, Jiang YL, et al. Exosomes from hypoxic urine-derived stem cells facilitate healing of diabetic wound by targeting SERPINE1 through miR-486-5p. *Biomaterials*. 2025;314:122893. doi:10.1016/j.biomaterials.2024.122893
25. Zhang W, Bao B, Jiang F, et al. Promoting oral mucosal wound healing with a hydrogel adhesive based on a phototriggered s-nitrosylation coupling reaction. *Adv Mater*. 2021;33(48):e2105667. doi:10.1002/adma.202105667
26. Fu YN, Li Y, Deng B, et al. Spatiotemporally dynamic therapy with shape-adaptive drug-gel for the improvement of tissue regeneration with ordered structure. *Bioact Mater*. 2021;8:165–176. doi:10.1016/j.bioactmat.2021.06.015
27. Liang Y, He J, Guo B. Functional hydrogels as wound dressing to enhance wound healing. *ACS Nano*. 2021;15(8):12687–12722. doi:10.1021/acsnano.1c04206
28. Fang W, Yang L, Chen Y, et al. Bioinspired multifunctional injectable hydrogel for hemostasis and infected wound management. *Acta Biomater*. 2023;161:50–66. doi:10.1016/j.actbio.2023.01.021
29. Jiang Y, Wang J, Zhang H, et al. Bio-inspired natural platelet hydrogels for wound healing. *Sci Bull*. 2022;67(17):1776–1784. doi:10.1016/j.scib.2022.07.032
30. Pan Y, Wang M, Wang P, et al. Effects of a semi-interpenetrating network hydrogel loaded with oridonin and DNase-I on the healing of chemoradiotherapy-induced oral mucositis. *Biomater Sci*. 2024;12(17):4452–4470. doi:10.1039/d4bm00114a
31. Hwang JH, Park YS, Kim HS, et al. Yam-derived exosome-like nanovesicles stimulate osteoblast formation and prevent osteoporosis in mice. *J Control Release*. 2023;355:184–198. doi:10.1016/j.jconrel.2023.01.071
32. Bligh EG, Dyer WJ. A rapid method of total lipid extraction and purification. *Can J Biochem Physiol*. 1959;37(8):911–917. doi:10.1139/o59-099
33. Hu C, Wei H, Hua B, et al. Facile fabrication of a broad-spectrum starch/poly(α-l-lysine) hydrogel adsorbent with thermal/pH-sensitive IPN structure through simultaneous dual-click strategy. *Carbohydr Polym*. 2023;309:120672. doi:10.1016/j.carbpol.2023.120672
34. Koide H, Okishima A, Hoshino Y, et al. Synthetic hydrogel nanoparticles for sepsis therapy. *Nat Commun*. 2021;12(1):5552. doi:10.1038/s41467-021-25847-2
35. Ou X, Wang H, Tie H, et al. Novel plant-derived exosome-like nanovesicles from Catharanthus roseus: preparation, characterization, and immunostimulatory effect via TNF-alpha/NF-kappaB/PU.1 axis. *J Nanobiotechnol*. 2023;21(1):160. doi:10.1186/s12951-023-01919-x
36. Seo K, Yoo JH, Kim J, et al. Ginseng-derived exosome-like nanovesicles extracted by sucrose gradient ultracentrifugation to inhibit osteoclast differentiation. *Nanoscale*. 2023;15(12):5798–5808. doi:10.1039/d2nr07018a
37. Jiang D, Li Z, Liu H, et al. Plant exosome-like nanovesicles derived from sesame leaves as carriers for luteolin delivery: molecular docking, stability and bioactivity. *Food Chem*. 2024;438:137963. doi:10.1016/j.foodchem.2023.137963
38. Wang F, Sun Q, Li Y, et al. Hydrogel encapsulating wormwood essential oil with broad-spectrum antibacterial and immunomodulatory properties for infected diabetic wound healing. *Adv Sci*. 2023;11:e2305078. doi: 10.1002/advs.202305078.
39. Xin X, Li J, Wu W, et al. ROS-scavenging nanomedicine for "multiple crosstalk" modulation in non-alcoholic fatty liver disease. *Biomater Sci*. 2023;11(10):3709–3725. doi:10.1039/d2bm02161g

40. Wang Z, Sun W, Hua R, et al. Promising Dawn in tumor microenvironment therapy: engineering oral bacteria. *Int J Oral Sci*. 2024;16(1):24. doi:10.1038/s41368-024-00282-3
41. Sedghi L, DiMassa V, Harrington A, et al. The oral microbiome: role of key organisms and complex networks in oral health and disease. *Periodontol 2000*. 2021;87(1):107–131. doi:10.1111/prd.12393
42. Sun J, Chen T, Zhao B, et al. Acceleration of oral wound healing under diabetes mellitus conditions using bioadhesive hydrogel. *ACS Appl Mater Interfaces*. 2022;15(1):416–431. doi:10.1021/acsami.2c17424
43. Baker JL, Mark Welch JL, Kauffman KM, et al. The oral microbiome: diversity, biogeography and human health. *Nat Rev Microbiol*. 2023;22(9):89–104. doi:10.1038/s41579-023-00963-6
44. Zhang Z, Zhang Q, Gao S, et al. Antibacterial, anti-inflammatory and wet-adhesive poly(ionic liquid)-based oral patch for the treatment of oral ulcers with bacterial infection. *Acta Biomater*. 2023;166:254–265. doi:10.1016/j.actbio.2023.05.017
45. Li Z, Liu J, Song J, et al. Multifunctional hydrogel-based engineered extracellular vesicles delivery for complicated wound healing. *Theranostics*. 2024;14(11):4198–4217. doi:10.7150/thno.97317
46. Zhao M, Wang C, Ji C, et al. Ascidian-inspired temperature-switchable hydrogels with antioxidant fullerenols for protecting radiation-induced oral mucositis and maintaining the homeostasis of oral microbiota. *Small*. 2023;19(27):e2206598. doi:10.1002/smll.202206598
47. Xiao H, Fan Y, Li Y, et al. Oral microbiota transplantation fights against head and neck radiotherapy-induced oral mucositis in mice. *Comput Struct Biotechnol*. 2021;19:5898–5910. doi:10.1016/j.csbj.2021.10.028
48. Dudding T, Haworth S, Lind PA, et al. Genome wide analysis for mouth ulcers identifies associations at immune regulatory loci. *Nat Commun*. 2019;10(1):1052. doi:10.1038/s41467-019-08923-6
49. De Ruysscher D, Faivre-Finn C, Nackaerts K, et al. Recommendation for supportive care in patients receiving concurrent chemotherapy and radiotherapy for lung cancer. *Ann Oncol*. 2020;31(1):41–49. doi:10.1016/j.annonc.2019.10.003
50. Douglass JD, Ness KM, Valdearcos M, et al. Obesity-associated microglial inflammatory activation paradoxically improves glucose tolerance. *Cell Metab*. 2023;35(9):1613–1629. doi:10.1016/j.cmet.2023.07.008
51. Wei Q, Su J, Meng S, et al. MiR-17-5p-engineered sEVs encapsulated in GelMA hydrogel facilitated diabetic wound healing by targeting PTEN and p21. *Adv Sci*. 2024;11:e2307761. doi:10.1002/advs.202307761.
52. Du X, Que W, Hu X, et al. Oridonin prolongs the survival of mouse cardiac allografts by attenuating the NF-κB/NLRP3 pathway. *Front Immunol*. 2021;12:719574. doi:10.3389/fimmu.2021.719574
53. Enzan N, Matsushima S, Ikeda S, et al. ZBP1 protects against mtDNA-induced myocardial inflammation in failing hearts. *Circ Res*. 2023;132(9):1110–1126. doi:10.1161/CIRCRESAHA.122.322227
54. Zhang Y, Wang T, Dong X, et al. Salivary amylase-responsive buccal tablets wipe out chemotherapy-rooted refractory oral mucositis. *Adv Sci*. 2024;11:e2308439. doi:10.1002/advs.202308439.
55. Diao Z, Li L, Zhou H, et al. Tannic acid and silicate-functionalized polyvinyl alcohol-hyaluronic acid hydrogel for infected diabetic wound healing. *Regen Biomater*. 2024;11:rbae053. doi:10.1093/rb/rbae053.
56. Jin J, Sun C, Xu K, et al. Multifunctional self-healing peptide hydrogel for wound healing. *Int J Biol Macromol*. 2024;261:129734. doi:10.1016/j.ijbiomac.2024